

## Recent Progress in Microscan Resolution Enhancement

William F. O'Neil

Northrop Grumman Corporation, Electronic Systems and Sensors Sector

P. O. Box 746 - MS G8

Baltimore, MD 21203-0746

### Abstract

*This paper presents experimental results for the Northrop Grumman resolution enhancement and non-uniformity correction algorithms. The results include simulation results using complex images, laboratory measurements of Modulation Transfer Function, Minimum Resolvable Temperature and Noise Equivalent Temperature Difference, and results obtained using microscanned flight data taken with a midwave IR staring sensor. The flight data includes urban and rural environments. These results show that resolution enhancement of greater than 2:1 has been achieved and is only limited by the optical resolution of the sensor. Non-uniformity correction without the use of calibration data is shown to reduce the fixed pattern offset noise to less than the temporal noise, even after temporal integration of multiple frames of data. Analytic models for the MTF are presented using two different assumptions regarding resolution enhancement. Comparison with the laboratory results shows that the effective detector size is reduced in addition to the expected effects of increase in sampling density.*

### Introduction

Microscanning has long been recognized as a technique for increasing the effective resolution of staring sensors. Prior work can be broadly classified into efforts that only considered the effect of increasing the sampling density to reduce aliasing caused by insufficient sampling of the spatial frequencies present at the image plane of the sensor, and efforts that attempted to recover the aliased spatial frequencies by combining the data from multiple frames of microscanned imagery. While both methods are technically feasible, several practical problems have restricted the use of these techniques. The primary problem is the computation costs when the scenes being microscanned are moving in an irregular fashion.

Several research efforts have developed sensors that provide an implicit computation using interlaced images from consecutive frames to achieve an "apparent" resolution enhancement of typically 2:1. These efforts usually take advantage of interlaced video displays coupled with eye-brain integration to provide increased Modulation Transfer Function (MTF) within the limits of detector aliasing. Aliasing caused by the finite detector aperture limits this method, even under static laboratory conditions. In a flight environment, the need for a known amount of interlace is very difficult to achieve. It can be argued that if the field of view of the

## Form SF298 Citation Data

<b>Report Date</b> <i>("DD MON YYYY")</i> 00001999	<b>Report Type</b> N/A	<b>Dates Covered (from... to)</b> <i>("DD MON YYYY")</i>
<b>Title and Subtitle</b> Recent Progress in Microscan Resolution Enhancement		<b>Contract or Grant Number</b>
		<b>Program Element Number</b>
<b>Authors</b>		<b>Project Number</b>
		<b>Task Number</b>
		<b>Work Unit Number</b>
<b>Performing Organization Name(s) and Address(es)</b> Northrop Grumman Corporation, Electronic Systems and Sensors Sector P. O. Box 746 - MS G8 Baltimore, MD 21203-0746		<b>Performing Organization Number(s)</b>
<b>Sponsoring/Monitoring Agency Name(s) and Address(es)</b>		<b>Monitoring Agency Acronym</b>
		<b>Monitoring Agency Report Number(s)</b>
<b>Distribution/Availability Statement</b> Approved for public release, distribution unlimited		
<b>Supplementary Notes</b>		
<b>Abstract</b>		
<b>Subject Terms</b>		
<b>Document Classification</b> unclassified		<b>Classification of SF298</b> unclassified
<b>Classification of Abstract</b> unclassified		<b>Limitation of Abstract</b> unlimited
<b>Number of Pages</b> 19		

sensor is small, and if the sensor is operated so as to stabilize the image on the focal plane, then the desired enhancement can be achieved. For the evolving distributed aperture imaging systems which have been our focus for several years<sup>1, 2, 3, 4, 5, 6</sup>, neither of these conditions obtain.

The second approach which we and others have been pursuing is to combine series of images to obtain both increased sampling density, and to separate the aliased frequency components, using them to reconstruct the higher spatial frequencies that are present at the image plane. The technical feasibility of this was shown using a Maximum Likelihood Estimator (MLE) algorithm<sup>7, 8, 9, 10</sup>. Their well known enhancement of static IR data is shown in Figure 1.

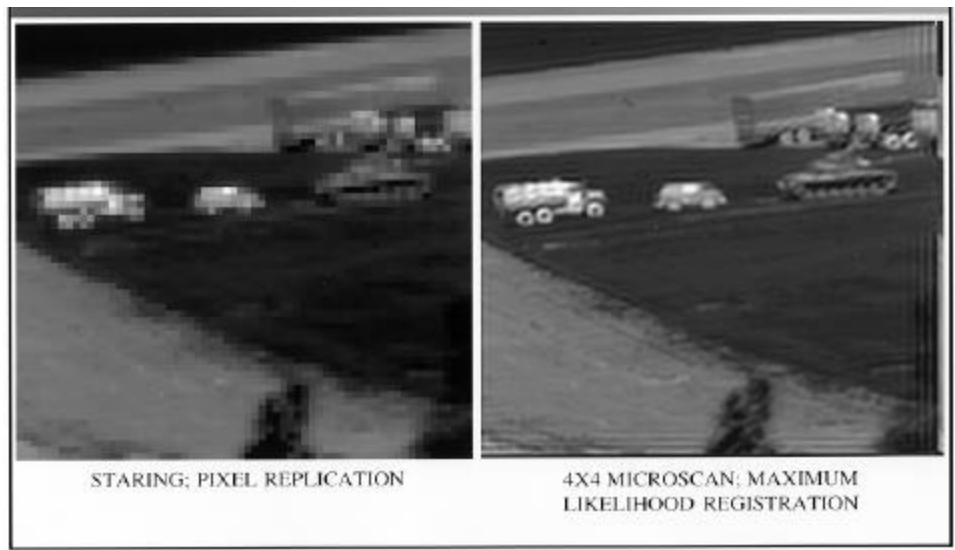


**Figure 1 – Resolution Enhancement Using Maximum Likelihood Method**

The images are taken with a 128x128 MWIR staring sensor. A series of 16 images was processed to achieve a 4:1 resolution enhancement shown in the right hand Image. Although the scene was static, this fact is not essential to the enhancement algorithm which they used. In fact, the sampling grid was not uniform due to an experimental problem, but the output image still contained frequency components beyond the detector limit of one cycle per detector aperture. The primary problem with this algorithm was the computational burden which could be as high as thousands of arithmetic operations per input sample. However, the strengths of the algorithm are very significant. There is no *a priori* assumption about the nature of the image, except that it is temporally invariant over the duration of the microscan sequence, and that it has finite energy. The excellent work by this group has been a major reason that we have continued to pursue resolution enhancement for the distributed aperture sensor system.

In this paper, the results of applying alternate algorithms that have some similarities to the Maximum Likelihood method will be presented. A major focus of this work is the reduction in computation costs. The very high payoff for increased resolution of distributed aperture sensors can be achieved if the costs for processing are containable within the resources of current and planned military aircraft. We have succeeded in reducing computation costs below 50 operations per input sample while achieving 2X resolution enhancements that are similar to the results from the MLE algorithm. This improves on the results reported in reference 11 by about 4:1. Of equal importance, the algorithms are shown to handle flight data and provide a degree of scene-based non-uniformity correction (NUC) not previously achieved. The paper describes four systems (two simulations and two experiments using actual sensor data) and compares the results with models that define the projected performance of the sensors when resolution enhancement and NUC are provided. The performance is compared with the performance predictions for an oversampled sensor as well as one in which the detector sizes are reduced to match the increased sampling density.

### **Resolution Enhancement Model**

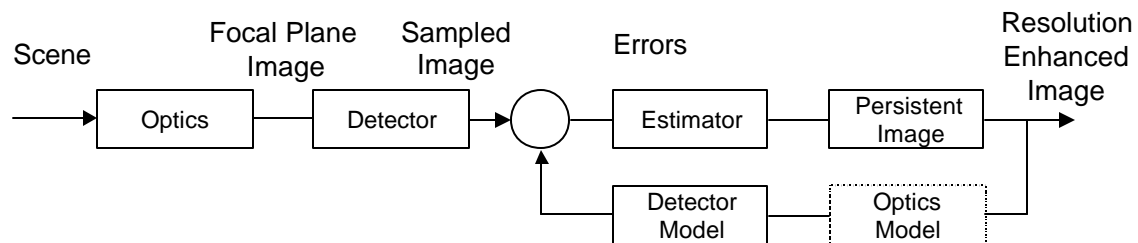


**Figure 2 – Estimating High Resolution Images**

The general form of the resolution enhancement model is shown in Figure 2. Scene data is modulated by the optics before arriving at the image plane as a two-dimensional image. The staring detector system samples this image using both a spatial sampling grid and the detector aperture function. Microscanning provides a series of sampled data sets at varying sample phases. If the scene is treated as a time invariant function, then the multiple data sets can be combined to obtain a single data set that has been sampled at higher sampling density. MLE takes this data set, and compares it with a set that is generated by the algorithm, then sampled in the same way that the detectors sampled the original image. The difference between the two data sets is used to refine the estimates of the individual data values using a recursive steepest descent method. In general, any component of the input image that modifies the detector data set when sampling phase is varied can be recovered in the output data set. Since the input data set is limited by the optics, the recoverable data is similarly limited. The sampling limits of the

detectors I have called the Nyquist Limit, while the optics limits I have designated the Rayleigh Limit.

Notice that we could close the estimation loop around an optics MTF which is equivalent to de-convolving the optics. However, spatial frequencies beyond the optics cut-off do not affect the scene presented to the detectors, and therefore cannot be recovered by this method. The usual techniques described in the literature for exceeding the Rayleigh Limit involve some statistical inference or other method of describing the necessary higher frequencies. One of the more successful methods has been the resolution of stellar binary objects where the existence of a binary pair is assumed in the enhancement process.

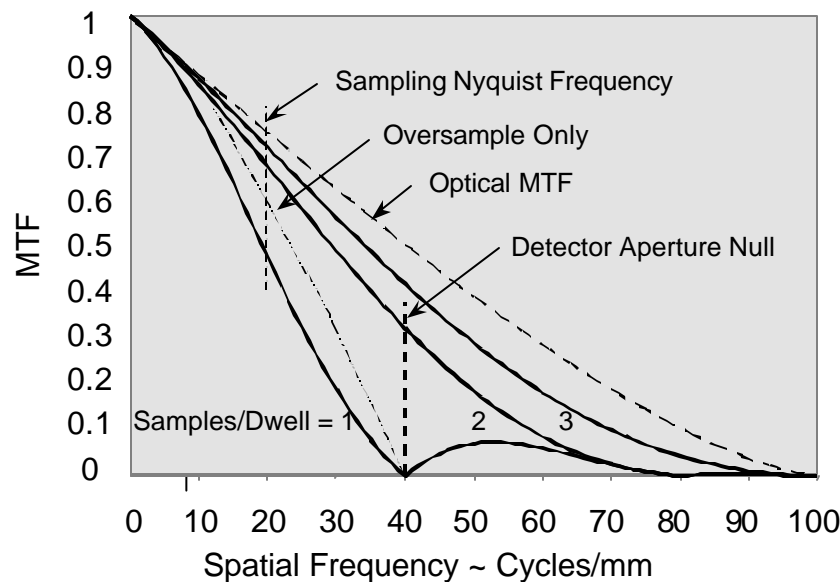


**Figure 3 – Effect of Detector Resolution Enhancement on MTF**

Figure 3 illustrates the trades for different algorithm choices. The Optics MTF for a Gaussian blur spot is the best available resolution for algorithms that operate only on detector data. A typical optics f# of 2.3 with diffraction-limited optics was assumed. The optical spatial frequencies extend to about 110 cycles per millimeter. To provide a Nyquist Frequency that exceeds the Rayleigh Limit requires detector sample spacing of 4.5 micrometers. This is much smaller than can be provided with current detector technology.

If the effect of a selected algorithm is to increase sample density without reducing the effective detector aperture, then the best available MTF is shown by the curve labeled 'Oversample Only'. When the effect of the algorithm is to reduce the effective aperture size, then the curves labeled 'Samples/Dwell = 1, 2, and 3' apply. The Nyquist Frequency is increased as sample density increases, and detector limits are also increased. It is this effective reduction in detector aperture that is

the primary attraction of the more complex MLE algorithms. The cases illustrated are for a 25 micrometer detector at a nominal wavelength of 4 micrometers.

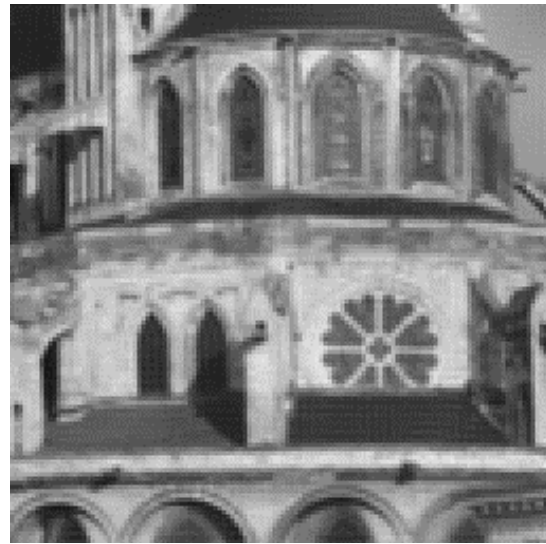
The experimental data that we have used was taken with arrays having detector spacing of 38 and 50 micrometers with operation in the MWIR band. For these two cases, the available resolution enhancement using MLE is 8.4:1 and 11:1 respectively. With conventional high resolution MWIR focal planes having 20-25 micrometer detectors, the available resolution enhancement is about 4.5-6:1 which is still a substantial increase.

### **Algorithm Simulation Results**

An algorithm simulation software platform was constructed for testing algorithms. This can accept either synthetic scenes or real images. To answer questions of enhancement accuracy, it typically uses a high resolution scene that is "scanned" by a simulated detector array to achieve a lower resolution. Intermediate resolutions are also available that match the degree of resolution enhancement that is being implemented. This permits direct comparison between the resolution achieved by an algorithm and the resolution that is provided by an "ideal" detector with the enhanced resolution. The simulation includes microscanning patterns and the ability to move the line of sight of the sensor in varying step sizes across the image. Addition of both fixed pattern noise and temporal noise is provided to permit evaluation of the ability to do NUC and to determine the ratio of output noise to input noise for both modes. A variety of scenes have been obtained by digitizing visible wavelength photographs. A typical source scene provides 1400x2000 pixels. Unenhanced detector array size is 64x64 elements with each detector covering a 4x4 array of source samples. Motion steps up to 5 detector elements per frame with a step size resolution of  $\frac{1}{4}$  detector element are provided. The platform runs under Windows 95. Using a 100 MHz Pentium laptop computer, the complete code, including detector simulation, resolution enhancement and display of 256x256 result images operates at about  $\frac{1}{2}$  frame per second. On a laboratory 350 MHz PC with better graphics, rates of 2.5 frames per second are obtained. There was no attempt to optimize this code for speed.



**Unenhanced Image**



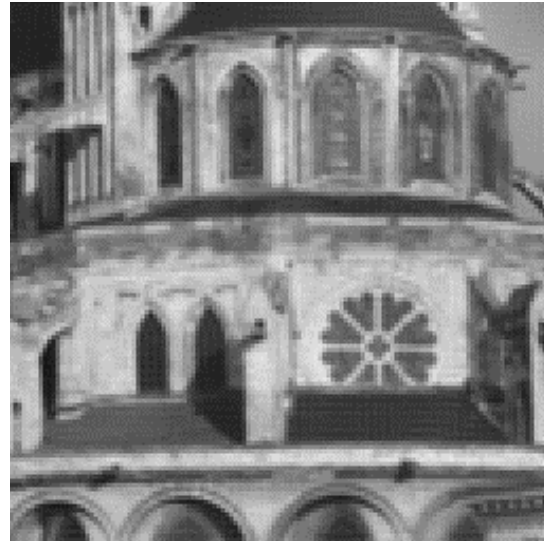
**2:1 Enhanced Image**

**Figure 4 – 2:1 Resolution Enhancement Simulation**

Figure 4 shows the source image at the detector resolution and the result of applying the enhancement algorithms using a 2:1 Microscan pattern. The source selected for this image is the Abbey L'homme in Caen, Normandy. It is used because it has a broad mixture of image patterns including repetitive lattices, smooth curves and a mixture of diagonal elements. In Figure 5, the enhancement of the detector image at a 2:1 enhancement ratio is compared with the ideal image that results when the source is sampled using a detector size that is 1/2 of the unenhanced detector size. The difference between these two images is not perceptible, but measurements show that the error in this noise-free case is about two percent of the signal.

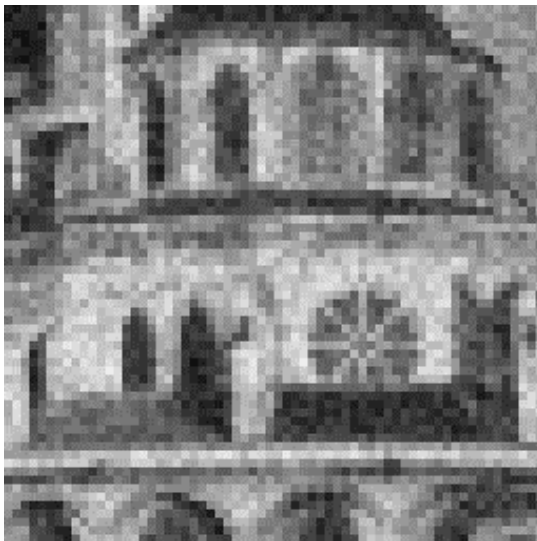


Ground Truth Image (Ideal)

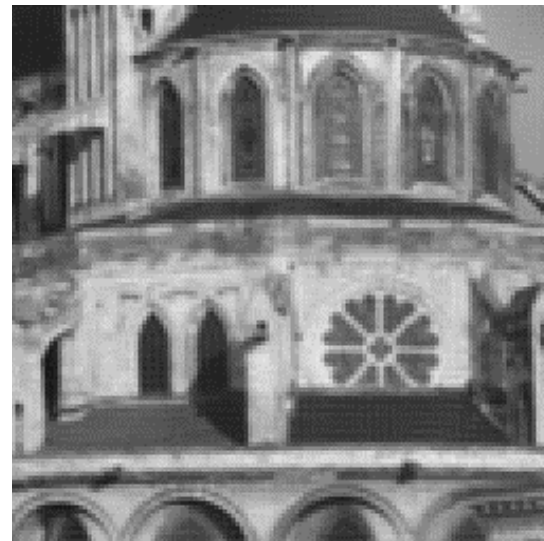


Enhanced Image

**Figure 5 – Comparison of Enhanced Image with Ground Truth Image**



Unenhanced Image + FPN



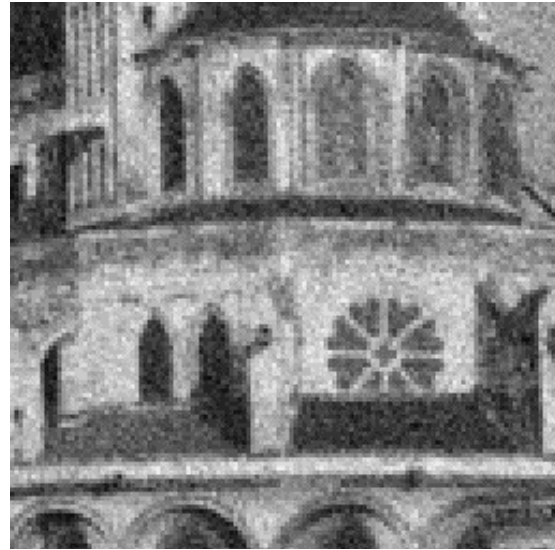
Enhanced Image

**Figure 6 – Enhancement Algorithm Eliminates Fixed Pattern Noise**

Figure 6 shows the addition of a large amount of fixed pattern noise to the detector image. The enhanced image has no discernible fixed pattern noise, due to the use of image gradients as a part of the enhancement algorithm structure. This is verified by the experimental results discussed below.



**Unenhanced Image + Temporal Noise**



**Enhanced Image**

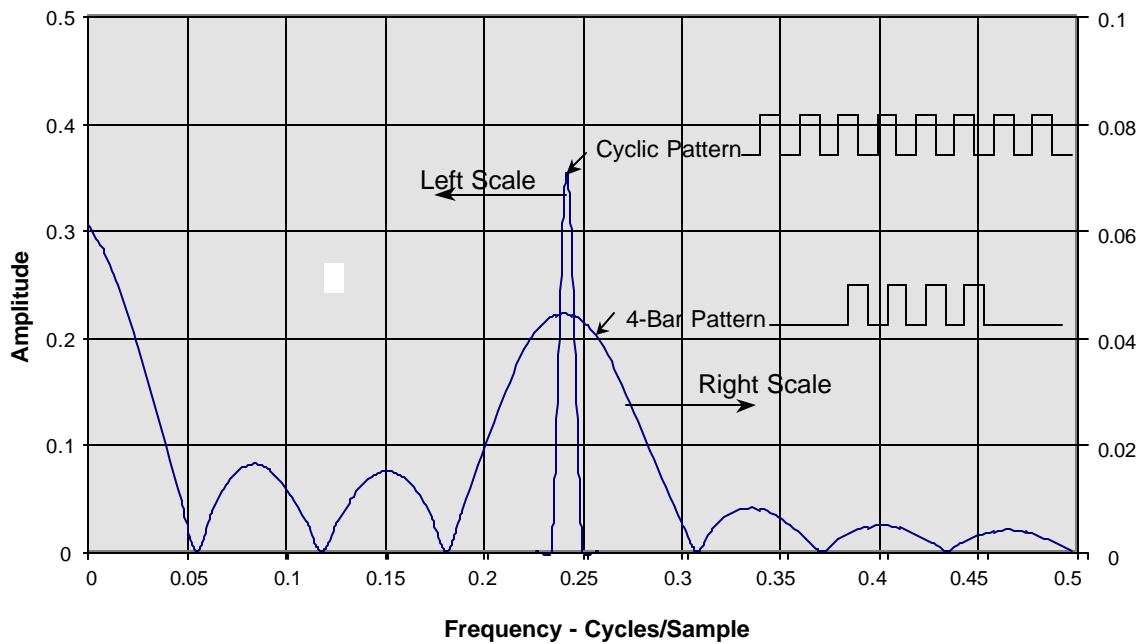
**Figure 7 – Temporal Noise is Unchanged by Enhancement Algorithm**

Figure 7 shows the addition of temporal noise only to the image, and the resulting enhanced image. Here the noise is visible on the output. The figure of merit is the ratio of sample noise on the output to sample noise on the input. For the particular form of the algorithms demonstrated here, the theoretical ratio is 1.06. The measured ratio is typically within ten percent of this value.

Since it is difficult to separate the visual content from the algorithm performance, this simulation was modified to show a standard 4-Bar target resolution enhancement. A specific point of interest is to show a case where the spatial frequency of the bars exactly matches the detector response null (one cycle per detector).

It is usual to refer to such targets as having a single spatial frequency. However, the spatial frequencies present in this target span a broad range of frequencies because of the portions that do not have the bars. Figure 8 shows the difference in spectra for a four bar target and for a repetitive square wave pattern extending over the entire field of view. The 4-Bar pattern that has bars and spaces that are two units wide for a total 4-Bar width of 14 units in a data series of 128 units. As expected the repetitive pattern has all of its energy concentrated at a single frequency. The 4-Bar target has its energy spread over the entire range of frequencies with relatively little at the 4-Bar “frequency”. The difference between these patterns determines the degree to which the 4-Bar series is aperiodic. A completely aperiodic series will exhibit a spectrum with uniform amplitude at each frequency. The reconstruction of the 4-Bar pattern is only in error by the amount that

signals near the 4-Bar frequency are lost. As noted above, for typical scenes, this is a small percentage error in reconstructing the high-resolution image.



**Figure 8 – Comparison of Single Frequency and 4-Bar Spectra**

Figure 9 shows the source image for the 4-Bar pattern. The simulated detector has a span of one 4-Bar cycle for the target below the right edge of the large target. Figure 10 shows the simulated unenhanced detector data compared with an ideal detector that is  $\frac{1}{2}$  the size in both dimensions. Figures 11 and 12 show the result of the enhancement algorithms for the best and worst sampling phase between the detectors and the image. When motion is added to microscanning, the effects of sampling phase can be discerned as a modulation of the amplitude for the target that is at the enhanced Nyquist Limit. This cannot readily be portrayed in static images but will be illustrated dynamically during the presentation. The key result from this simulation is the ability to derive signals at the detector null provided that they are immersed in an aperiodic sequence. However, it is also notable that signals having spatial frequency content beyond the detector null are also recovered, including signals at the second detector null. Of course, in this simulation there is no Rayleigh Limit to contend with as the high resolution signals were generated analytically.

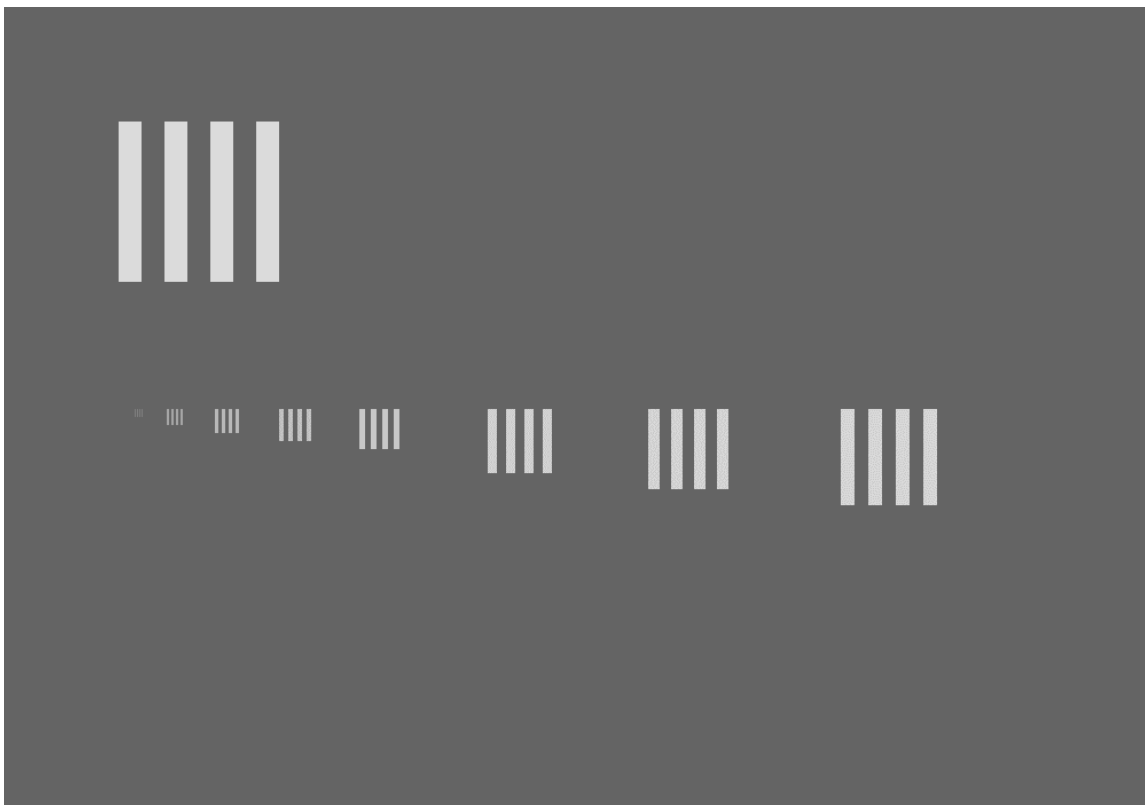
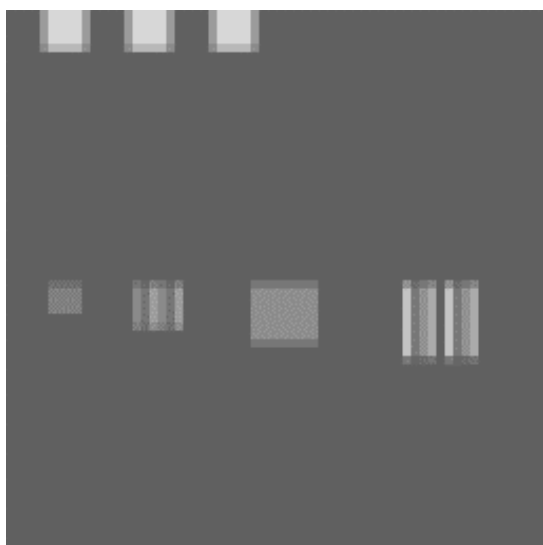
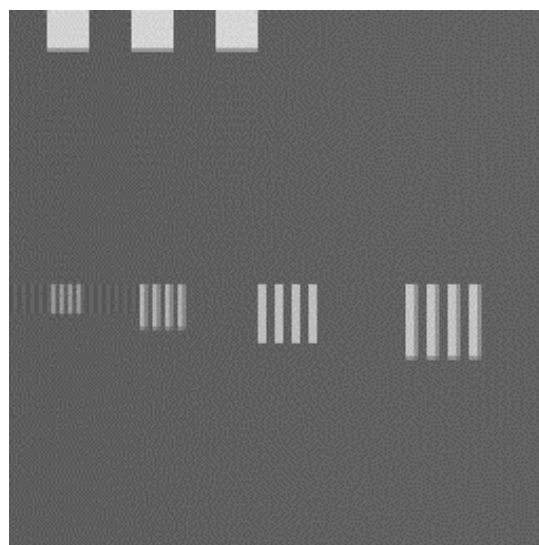


**Figure 9 – Simulated 4-Bar Targets with Periods Matched to Detector Size**

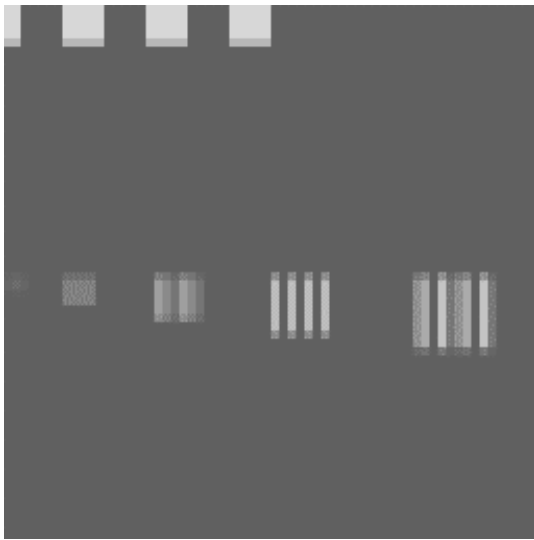


Unenhanced Image

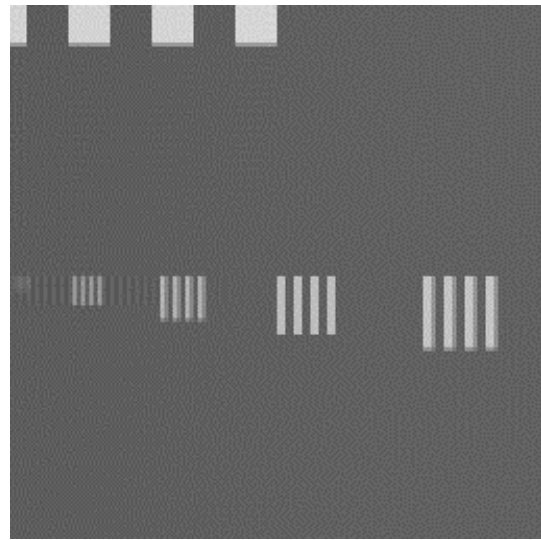


Ideal Ground Truth Image

**Figure 10 – Unenhanced 4-Bar Images vs. Ideal 2X Enhanced Images**

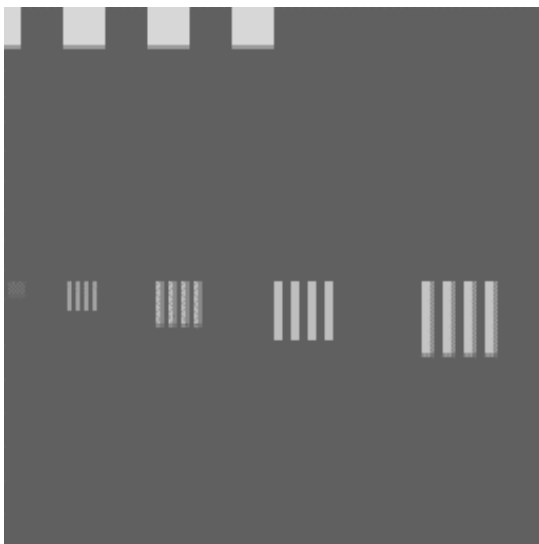


Enhanced Image

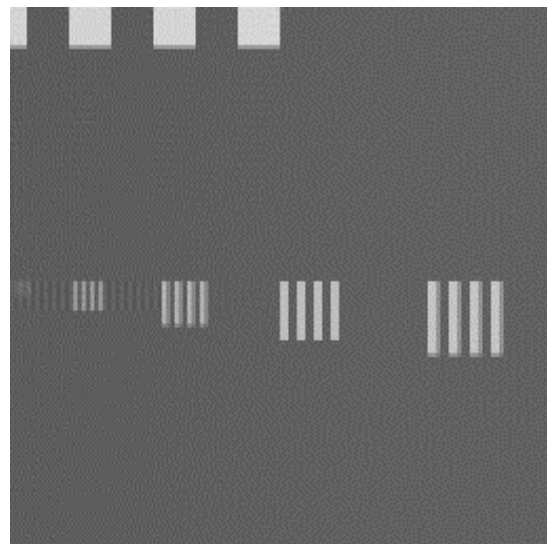


Ideal Ground Truth Image

**Figure 11 – Enhanced 4-Bar Images at Poorest Sampling Phase (Alias Canceling)**



Enhanced Image



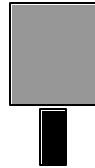
Ideal Ground Truth Image

**Figure 12 – Enhanced 4-Bar Images at Best Sampling Phase (Alias Adding)**

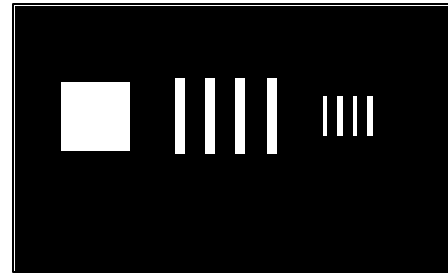
## Laboratory Experimental Results



Radiance  
Camera



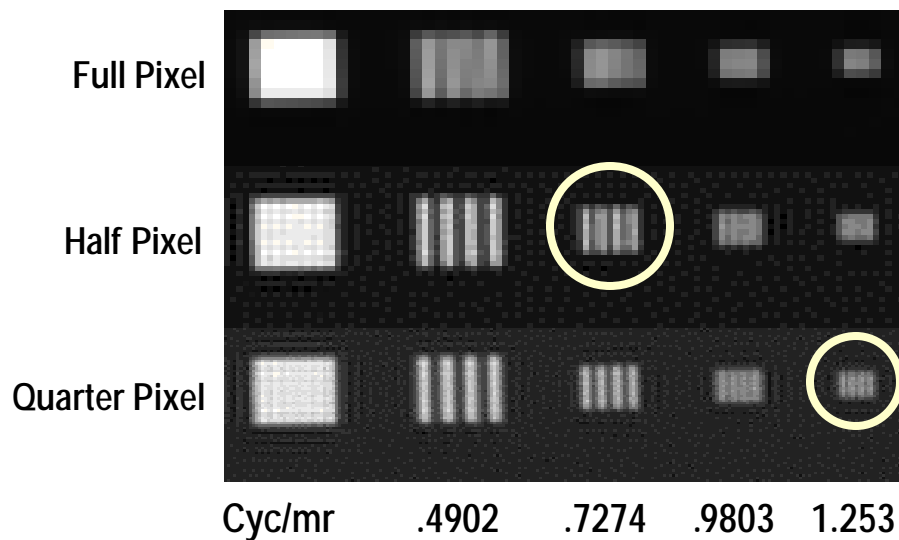
Dither  
Mirror



Blackbody w/  
bar patterns

**Figure 13 – DAIRS Laboratory Algorithm Verification Equipment**

The algorithms have been transferred to the Distributed Aperture IR Sensor (DAIRS) laboratory (Figure 13). The sensor for these experiments is the Amber Radiance I camera with 256x256 detectors. The laboratory tests have included measurements of MTF, MRTD and NUC, plus error measurements of scene-based motion measurement algorithms. MTF was determined using the digital data such as that shown in Figure 14. Selected rows were analyzed using Mathcad to determine modulation. Maximum, minimum and average excursions were determined for multiple instances.



Amber Radiance I w/o Microscan, 38m, 25mm fl  
 $\text{Nyquist frequency} = \text{fl}/(2d) = 25/(2 \times 38) = .328 \text{ cy/mr}$

November 1997 results

**Figure 14 – Laboratory Tests Verify Resolution Enhancement**

The 2X enhancement cases (Half Pixel microscan) were analyzed using single horizontal data lines and are plotted in Figure 15 which also compares these results with MTF models using two different assumptions. The Interlaced Model assumes that the sample density is increased by 2X while the detector aperture is unchanged. The Maximum Likelihood (MLE) Model assumes that the sample density is increased by 2X and that the detector aperture is halved. The lowest curve shows the unenhanced prediction, the middle curve shows the Interlaced Model prediction, and the upper curve shows the MLE Model prediction. Actual data is between the upper and middle curves, but extends to frequencies well beyond Nyquist as is expected from the composite image shown in Figure 14. It is clear that the measured MTF routinely exceeds the predicted MTF for the Interlaced Model. The observed deficit relative to the MLE Model prediction has not been explained, but may be due to non-ideal detectors or optics.

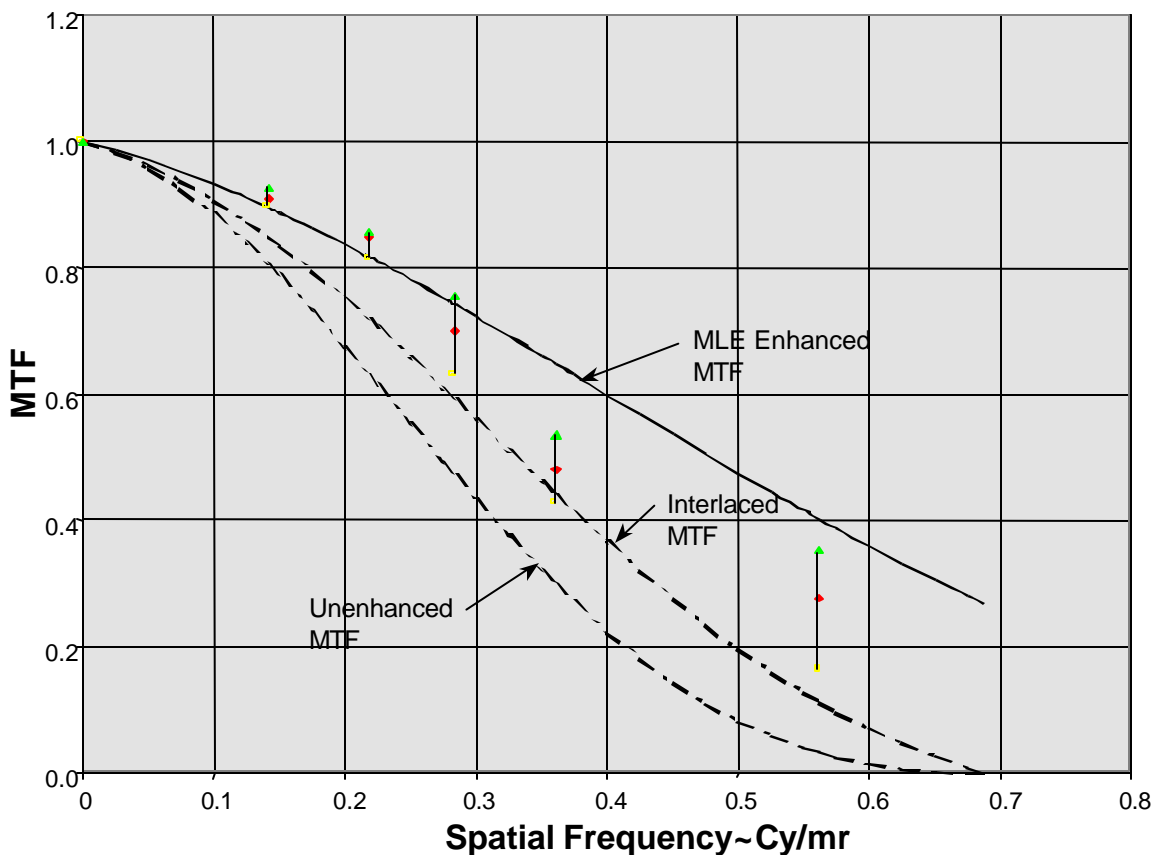


**Figure 15 – Comparison of Experimental MTF with Two Models**

Measurement of MRTD uses a conventional arrangement of 4-Bar targets with a calibrated source. Temperature difference is controlled to obtain transitions from visible to not visible and vice versa for both colder and hotter than background transitions. Multiple observers and multiple sequences with each observer were

used. To provide the 30 Hz frame rate needed for correct eye integration, the size of each frame has been reduced to allow use of a standard Sun work station as the driver. Figure 16 shows the MRTD results for one observer with unenhanced and 2:1 resolution enhancement images.

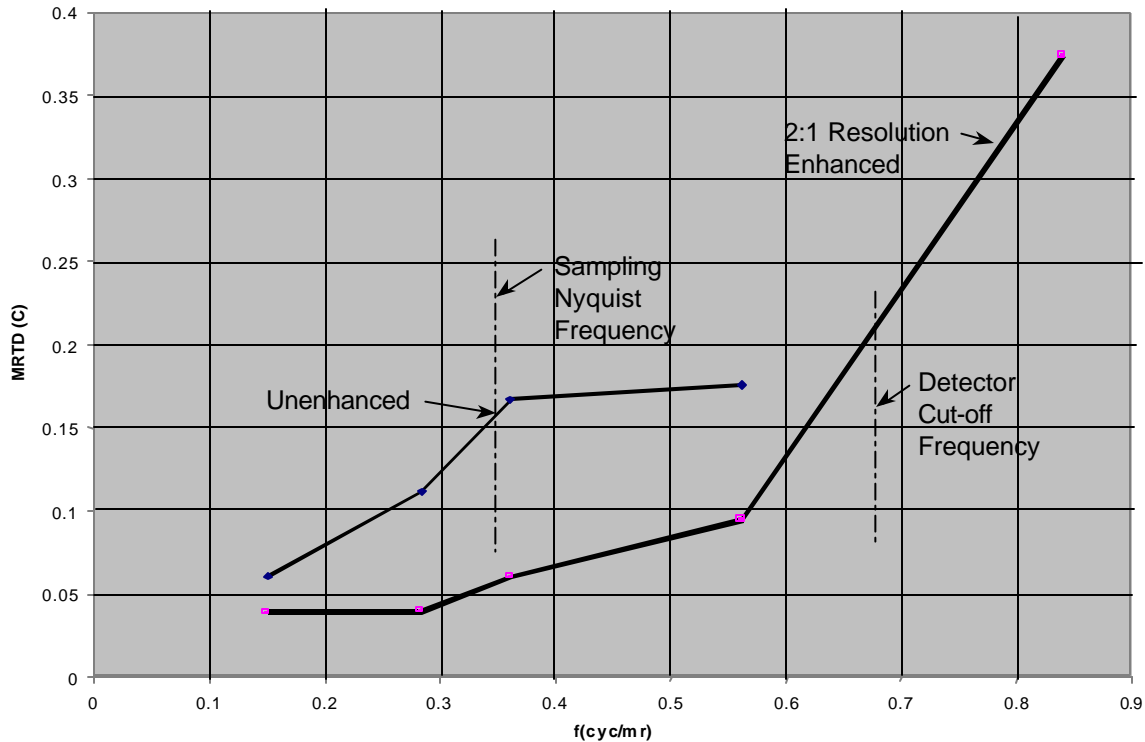


**Figure 16 –Measured MRTD**

As a part of the diagnosis of the MTF deficit, measurements of the ability to determine microscan motion from scene data were repeated in the laboratory. The error between measured displacement and scene based estimated displacement has a standard deviation of less than 0.01 detector IFOV, but does exhibit a scale factor bias of about 5% which is being investigated. The measurement method did not provide information concerning absolute registration. For resolution enhancement algorithms of the MLE type, the short term repeatability is the main error of concern. Methods from the open literature<sup>12</sup>, suggest poorer results than obtained here, but those methods do not include corrections for errors caused by aliasing and fixed pattern noise.

The algorithms use the detector difference operator for NUC which has been presented in prior papers<sup>4, 6</sup>. For convenience, the equations are repeated here. If we have two sets of data from detectors with the same offsets, then we can eliminate the offset by subtracting one set from the other set. If the detectors are looking at the same scene location, we will also remove the scene signal. When

microscanning, or otherwise moving the line of sight, the detector differences will contain scene differences without offsets. For any detector:

$$D_1 = S_1 + \text{Offset}_1$$

$$D_2 = S_2 + \text{Offset}_2$$

$$\text{But } \text{Offset}_1 \circ \text{Offset}_2 \circ \text{Offset}$$

$$D_2 - D_1 = S_2 - S_1 + \text{Offset} - \text{Offset} = S_2 - S_1$$

Notice that there is no need to estimate the offset or perform any added arithmetic to remove it. The resulting signals are spatial differences which are used to reconstruct the intensity image. The primary draw back of this approach is the need to know the positions of the two signals for purposes of reconstruction. In the case of resolution enhancement, such knowledge is essential for MLE class algorithms and can be derived using the MLE approach.

A definitive test for NUC is to perform frame integration over a large number of frames, and to plot the total noise versus number of frames. When the noise is purely temporal (uncorrelated from frame to frame), the total noise will increase proportional to the square root of the number of frames integrated, while the sensitivity will increase proportional to the number of frames. Thus, the NETD will decrease proportional to the inverse of the square root of the number of frames as shown in Figure 17. The experimental data shown in the figure indicates that the fixed pattern noise is reduced to less than 2-3 percent of temporal noise and can be interpreted as validating reduction of fixed pattern noise to zero as predicted by the equations above.

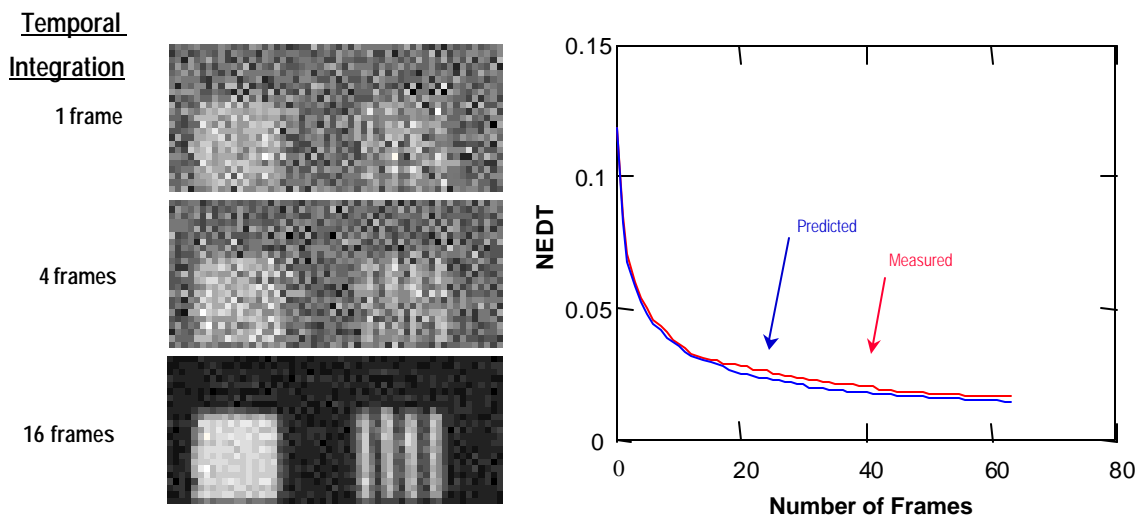


**Figure 17 – Frame Integration Test Confirms NUC Prediction**

## **Flight Data Analysis**

A prior internally-funded program flew a prototype sensor with a 128x128 InSb array. The sensor used a 25 mm lens with f# 2.3. Detector size was 50x50 micrometers nominal. Sensor data was collected as 12 bit samples at a frame rate of 60 Hz. Microscan motion was provided by a mirror driven by a commercial piezo-electric actuator. Typical frame integration time was about one millisecond. Cooling was provided by an LN<sub>2</sub> pour dewar which was vented to the atmosphere. The sensor was flown on a BAC 1-11 used at our Baltimore facility for a variety of experimental programs. Calibration was performed immediately prior to each flight using external equipment. Variations in LN<sub>2</sub> temperature were caused by altitude changes. These, in turn caused large variations from the calibrated fixed pattern noise.

The algorithms used in the laboratory have been adapted for analysis of this flight data. The primary changes are the need to incorporate an optical flow model that allows image motion to vary over the field of view. This change adds a significant computational burden, but has been successfully demonstrated to recover flight scene motions within about .025 source samples ( $1\sigma$ ). A variety of error sources have been identified and corrected to achieve this result. The motion history for a short segment of flight data is shown in Figure 18. The nominal microscan motion is a square measuring one-half source pixel in each direction. There was no in flight measurement due to the nature of the equipment used to drive the microscanner. The commanded position was recorded.

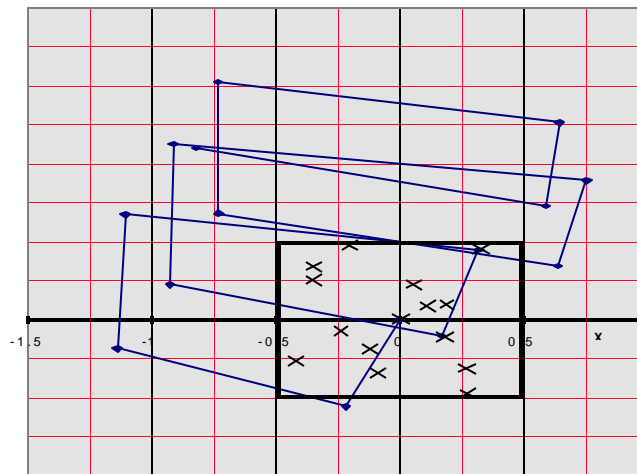


**Figure 18 – Flight Data Motion Estimates**

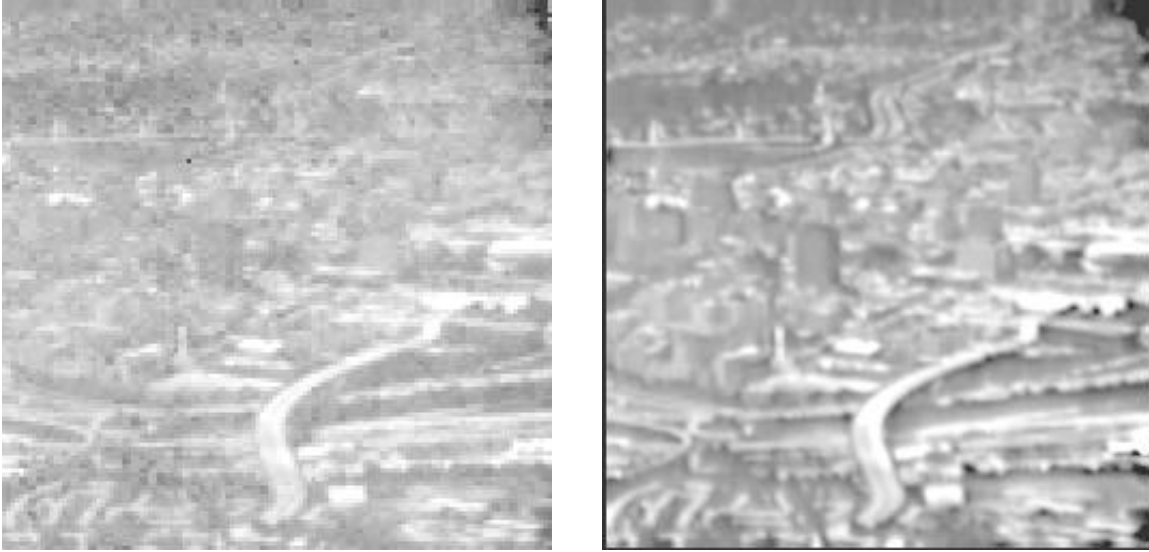


**Figure 19 – Flight Data Showing Resolution Enhancement and NUC**

Figure 19 illustrates the resolution enhancement and NUC achieved with the flight data. The non-uniformity is fully corrected without use of any offset calibration table. The white spot at the lower right edge is caused by a group of bad detectors that flashed irregularly from zero to full scale. To assess the resolution enhancement separate from the non-uniformity correction, the enhanced image has been resampled to the detector resolution. Figure 20 compares the resampled image with the enhanced image. The loss of detail in the original image was clearly impacted by the large fixed pattern noise. There is still a significant improvement in image quality.

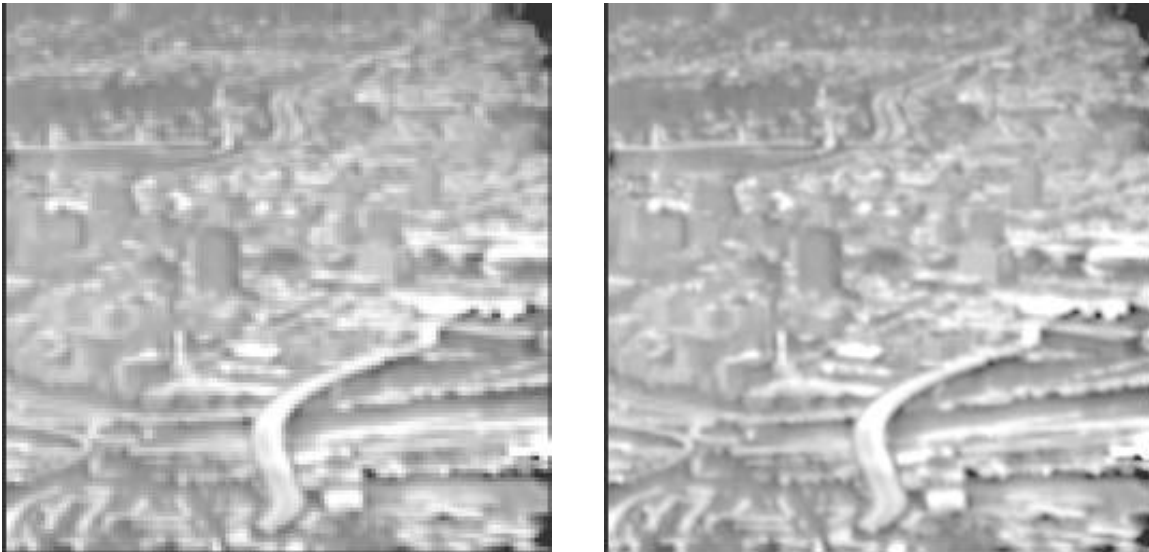


**Figure 20 – Comparison of Enhanced Image with Simulated Source**

## **Conclusions**

Algorithms have been developed that provide Resolution Enhancement, Non-uniformity Correction and Sensitivity Enhancement using microscanned IR images. The algorithms differ from prior efforts primarily in speed. This speed improvement provides a path to a real time application of these techniques which will significantly improve the performance of imaging sensors. The performance of the algorithms has been verified using simulated data and real sensor data from both laboratory and flight. Laboratory tests have confirmed the analytic models used to predict the performance of these enhanced images.

## **Acknowledgments:**

The Distributed Aperture Infrared System (DAIRS) Program is funded by the Office of Naval Research, Dr. Jim Buss, sponsor with Harvey Sokoloff of NAWC/AD as the Program Monitor. Steve Campana, Al Blumenthal and Nancy MacMeekin have been active participants in the technical reviews. The algorithm efforts reported here, together with some of the laboratory efforts were funded by Northrop Grumman, The DAIRS Program has provided the balance of the experimental effort funds. The internal company support is due to the efforts of Bob Hale and Ted Foster

The DAIRS Program Manager is Tom Brusgard. The laboratory efforts have been under the direction of Doug Ferguson with the assistance of Saleem Wali, Frank Kaisler, Dr. Marty Woolfson, Steve Gottesman and Jim Weygandt.

A Cooperative Research and Development Agreement with the Wright Aeronautical Laboratory team directed by Brian Yasuda has provided direct access to data and also interactive reviews that bring their expertise to bear on this project.

The continued interaction with the many people cited above has been key to the advancement of this project. The author wishes to acknowledge the contributions that they have made to clarifying the concepts and providing a patient forum for the ideas that have been developed.

## **References:**

1. R. A. Hale et al - United States Patent No. 5,317,394 "Distributed Aperture Imaging and Tracking System" issued May 31, 1994
2. R. A. Hale et al - United States Patent No. 5,412,421 "Motion Compensated Sensor" issued May 2, 1995
3. W.F. O'Neil, "Adaptive Spectrum Control", 1992 meeting of the IRIS Specialty Group on Passive Sensors
4. W.F. O'Neil, "D.C. Restoration of Common Module FLIRs", 1992 meeting of the IRIS Specialty Group on Passive Sensors

5. W. F. O'Neil, "Experimental Performance of a Dither-Scanned InSb Array", 1993 meeting of the IRIS Specialty Group on Passive Sensors
6. W. F. O'Neil, "Experimental Verification of Dither Scan Non-uniformity Correction", 1996 meeting of the IRIS Specialty Group on Passive Sensors
7. E. Watson, R. Muse, and F. Blommel, "Aliasing and Blurring in Microscanned Imagery" SPIE 1992
8. S. Cain, R. C. Hardie, and E. Armstrong, "Reconstruction of Aliased Video Sequences Via a Maximum-Likelihood Approach" IEEE Transactions on Image Processing 1995 and IRIS Specialty Group on Passive Sensors 1996
9. E. Kaltenbacher and R. C. Hardie, "Registration and High Resolution Reconstruction of Multi-Frame, Low Resolution, Aliased Infrared Images" – SPIE Aerosense 1996 and NAECON 1996
10. R. C. Hardie and E. Kaltenbacher, "High Resolution Infrared Image Reconstruction using Multiple, Low Resolution, Aliased Frames" - to be published
11. W. F. O'Neil, "Processing Requirements for the First Electro-Optic System of the Twenty-First Century" – AIAA/IEEE Digital Avionics System Conference, Oct. 26-30, 1997
12. A. Schaum, and M. McHugh, "Analytic Methods of Image Registration: Displacement Estimation and Resampling", NRL Report 9298, Feb. 28, 1991